Origins of bandgap bowing in compound-semiconductor common-cation ternary alloys

2009 J. Phys.: Condens. Matter 21 075802

(http://iopscience.iop.org/0953-8984/21/7/075802)

J. Phys.: Condens. Matter **21** (2009) 075802 (6pp) doi:10.1088/0953-8984/21/7/075802

Origins of bandgap bowing in compound-semiconductor common-cation ternary alloys

Nacir Tit[1,3], Ihab M Obaidat[1] and Hussain Alawadhi[2]

[1] Department of Physics, UAE University, PO Box 17551, Al-Ain, United Arab Emirates
[2] Department of Applied Physics, University of Sharjah, PO Box 27272, Sharjah, United Arab Emirates

E-mail: ntit@uaeu.ac.ae

Received 28 October 2008, in final form 18 December 2008
Published 29 January 2009
Online at stacks.iop.org/JPhysCM/21/075802

Abstract

We present an investigation into the existence and origins of bandgap bowing in compound-semiconductor common-cation ternary alloys. As examples, we consider $CdSe_xTe_{1-x}$ and $ZnSe_{1-x}Te_x$ alloys. A calculation, based on the sp^3s^* tight-binding method including spin–orbit coupling within the framework of the virtual crystal approximation, is employed to determine the bandgap energy, local density of states and atomic charge states versus composition and valence-band offset. The results show that (i) in the valence band, the top states are mainly contributed by Te atoms. The degree of ionicity of all atoms is found to vary linearly with mole fraction x. (ii) There is a strong competition between the anions (Se and Te) in trapping/losing charges and this competition is the main reason for the bandgap bowing character. (iii) There is a reasonable agreement between the calculated results and the available photoluminescence data. (iv) The bowing parameter is found to increase with increasing valence-band offset and increasing lattice mismatch.

1. Introduction

In the last two decades, II–VI semiconductor ternary and quaternary alloys have attracted a lot of attention because of their potential use in optoelectronic devices operating in the visible spectral range [1]. In particular, Zn(Cd)Se(Te) alloys have been the subject of many investigations for several reasons: (i) they possess a range of *direct* bandgaps covering most of the visible spectrum from near-infrared to ultraviolet [2]; (ii) they are characterized by bright emissions; (iii) lattice constants of ZnSe and CdSe match those of GaAs and InAs, respectively, which are popularly used as substrates; (iv) ZnSe is commonly used as a buffer on GaAs because it has a *direct* and large bandgap lying within the blue spectral region [3, 4]. The achievement of p-doping of ZnSe in 1991 raised further interest in it.

However, despite decades of extensive studies, there is no commonly accepted explanation of the origin of the widely observed nonlinear dependence of the fundamental bandgap with the alloy composition. The composition dependence of the bandgap is usually described by a second-order polynomial with the quadratic term proportional to the so-called *bowing* parameter [5]. In one treatment of this subject, it is argued that the bowing parameter can be decomposed into three parts originating from charge exchange, volume deformation, and structural relaxation [6]. But in this theory, it is also assumed that a single bowing parameter can describe the bandgap behavior in the whole composition range. This assumption is based upon the validity of the virtual crystal approximation (VCA). But, in the case of highly mismatched alloys, such as $IIIV_{1-x}N_x$ materials, the N-induced bandgap reduction and the greatly reduced pressure dependence of the bandgap in these alloys significantly deviate from the VCA-based predictions. It has been demonstrated that the composition dependence of the bandgap for these alloys cannot be described using a single bowing parameter. A band-anticrossing model has been developed to explain these unusual effects [7].

On the computational side, different methods have been used in the calculation of the electronic band structures of alloys. However, many were limited either by the system

[3] Author to whom any correspondence should be addressed.

size and the applicability only for ground-state properties (with underestimation of bandgap energy), such as the first-principles methods, or the complete neglect of the band-mixing effects, such as the Hückel method and the effective-mass approach (based on the Kronig–Penney model). To overcome such difficulties, we have used the sp^3s^* tight-binding (TB) method with inclusion of spin–orbit interactions [8, 9], which are important for the case of II–VI materials like those presented in this work. The TB method has shown its reliability in successfully simulating the experimental data while incorporating the microscopic description of the material by including the point-group symmetry of the system. Within the Slater–Koster scheme [9], the TB method uses a small basis set of atomic orbitals and this gives the method the ability to deal with large systems; meanwhile, it takes into account the band-mixing effects that are essential in the band structure of systems such as alloys.

Traditionally, and because of its simplicity, the VCA is usually preferred for the treatment of chemical disorder in semiconductor alloys. In the VCA, the potential of each atom in the alloy is replaced by a weighted average of the potentials of its components. It does lead to a qualitative explanation of most of the features in the bandgap bowing of the alloy. Unfortunately, in systems where large atomic relaxations and reconstructions take place, the VCA vastly underestimates the bowing of the bandgap.

In another related investigation, García and co-workers [10] have shown in their TB calculations on the $Zn_{1-y}Cd_ySe_{1-x}Te_x$ and $Zn_{1-y}Cd_yS_{1-x}Se_x$ quaternary alloys that the bandgap energy possesses a bowing character when the mole fraction of anions (x) is varied and, on the other hand, it follows an almost linear variation when the composition of cations (y) is varied. Similar bowing and linear behaviors were also reported in the experimental work of Seong and co-workers [11] on the common-cation and common-anion II–VI ZnTe-based alloys. These behaviors were corroborated in the theoretical simulations of El-Haj Hassan and co-workers [12] using the density-functional theory (DFT) and Charifi and co-workers [13] using the linearized-augmented plane wave (LAPW) method. Nonetheless, the origin of bandgap bowing is still an open question. In the present work, we use the tight-binding method with the inclusion of spin–orbit coupling [14] to investigate the existence and the origin of the bowing behavior in two cases of common-cation ternary alloys ($CdSe_xTe_{1-x}$ and $ZnSe_{1-x}Te_x$). The calculated results of bandgap energies are also fitted to the available photoluminescence (PL) data.

This paper is organized as follows. The next section gives some details of the TB models and method. In section 3 we discuss our calculated results and compare them to experimental data. The last section (section 4) summarizes our main findings and conclusions.

2. Computational method

Within the TB framework, atomic levels and electronic-interaction integrals are taken as adjustable parameters in order to fit the experimental or the first-principles band structures. Vögl *et al* [15] have proposed a nearest-neighbor TB description of IV and III–V semiconductors using the sp^3s^* basis set. In their work, the actual Hamiltonian is replaced with a pseudo-Hamiltonian which involves five orbitals per atom: s and 3p orbitals to describe the sp^3 hybridization and one excited s^* orbital, whose function is to provide a better description of the lowest unoccupied energy levels (low-lying conduction bands (CBs)). The first extension to further incorporate the spin–orbit coupling within the TB framework was done for II–VI semiconductors, even prior to Vögl's work, by Kobayashi *et al* [8], namely on CdTe and HgTe. In these materials, the spin–orbit splitting is quite strong and its successful incorporation into the TB Hamiltonian has paved the way for a large field of applications, especially in the area of II–VI semiconductors.

Table 1. The variation of bowing parameter 'b' with lattice mismatch ($\Delta a/a_0$) and VBO in the studied alloys.

Alloy	$\Delta a/a_0$	VBO (eV)	b (eV)
CdSeTe	6.8%	0.57[a]	0.904[b], 0.916[c]
ZnSeTe	7.3%	0.73[a]	2.185[b], 1.413[d], 1.239[e], 1.285[f]

[a] Reference [17]. [b] Present work. [c] Reference [19].
[d] Reference [11]. [e] Reference [21]. [f] Reference [22].

Moreover, in the supercell calculations the validity of two main points is assumed: (i) the virtual crystal approximation (VCA) in evaluating the supercell atomic structure and (ii) the problem of energy reference between the alloy constituents is sorted out by taking the valence-band offset (VBO) into account within the scheme of VCA [16]. For instance, the valence-band edge of CdTe stands higher in energy than the one of CdSe when an interface is formed between these two materials [17] such as the case of a free-standing heterostructure (i.e. VBO $= E_v(\mathrm{CdTe}) - E_v(\mathrm{CdSe}) \geqslant 0$). Consistent with this and with the VCA principle to take an average potential, in the case of $CdSe_xTe_{1-x}$ alloy, each Te atom is bonded to four Cd atoms. Thus, all the Te on-site energy elements should be shifted by a VBO value. However, each Cd atom is four-fold coordinated with the x fraction to be Se and the $(1-x)$ fraction to be Te. So, the Cd on-site energy elements should be shifted by $(1-x) \times$ VBO with respect to the bulk values. The VBO values were originally calculated by Wei and Zunger [17] using the first-principles all-electron band-structure method and are listed among the data presented in table 1.

In the present work, we use the empirical TB parameters of Olguín and Baquero [14], which yield excellent fittings to the experimental bandgap energies and carrier effective masses. The TB Hamiltonian matrix elements are expressed in a basis of symmetrically orthonormalized atomic orbitals $|a, \mu, \mathbf{R_i}\rangle$ (the so-called Löwdin orbitals [9]), where $\mathbf{R_i}$ denotes a Bravais lattice point referring to the primitive cell, a is a basis atom in the primitive cell and μ denotes an orbital (such as $|s, \frac{1}{2}\rangle$ as an eigenstate of the total-angular momentum $\mathbf{J} = \mathbf{L} + \mathbf{S}$) on atom a. The Hamiltonian is usually expressed [8] in terms of a basis $|a, \mu, \mathbf{k}\rangle$, which is obtained via a discrete Fourier

transformation of the localized orbitals $|a, \mu, \mathbf{R_i}\rangle$, and given by

$$|a, \mu, \mathbf{k}\rangle = \frac{1}{N_w} \sum_j e^{i\mathbf{k}\cdot\mathbf{R_j}} |a, \mu, \mathbf{R_j}\rangle \quad (1)$$

where $\mathbf{k}$ is a wavevector, usually taken either from within the irreducible wedge (IW) of the Brillouin zone if the aim is to calculate the density of states, or along the high-symmetry lines if the aim is to calculate the bands; N_w is the number of $\mathbf{k}$-vectors taken from within the IW.

With the inclusion of the spin–orbit interaction, the sp^3s^*-TB Hamiltonian is expressed in the Löwdin basis set (denoted below as $|i, \mu\rangle \equiv |a, \mu, \mathbf{R_i}\rangle$ for simplicity) as follows:

$$H = \sum_{i,\mu} |i, \mu\rangle E_{i,\mu} \langle i, \mu| + \sum_{i,\mu;\, j,\nu (i \neq j)} |j, \nu\rangle U_{i\mu,j\nu} e^{i\vec{k}(\vec{r}_j - \vec{r}_i)} \langle i, \mu| \quad (2)$$

where i and j refer to atoms at the respective positions $\vec{r}_i$ and $\vec{r}_j$; μ and ν refer to one of the ten orbitals on the atom i and j, respectively; $E_{i,\mu}$ is an on-site (diagonal) energy element of orbital μ for site i; $U_{i\mu,j\nu}$ is the overlap integral between the indicated respective orbitals. For further details of the expressions for the overlap integrals, we refer the reader to [8]. The TB parameters are obtained from [14].

The Bloch wavefunction $|n, \mathbf{k}\rangle$, of course, should diagonalize the TB Hamiltonian and is written as

$$H|n, \mathbf{k}\rangle = E_{nk}|n, \mathbf{k}\rangle \quad (3)$$

where n is a band index; E_{nk} is the eigen-energy corresponding to the eigen-vector (Bloch wavefunction). In our particular case of ternary alloys, both constituents possess *direct* bandgaps at the Γ-point. So, except for band structure or density of states calculations, the bandgap energy (E_g) is calculated only at the Γ-point.

The obtained eigen-energies $E_{n\mathbf{k}}$ and corresponding eigen-functions $|n, \mathbf{k}\rangle$ are used to calculate the following quantities:

(i) the total density of states (TDOS) given by

$$N(E) = \frac{1}{N_w} \sum_{n,\mathbf{k}}^{N_w} \delta(E - E_{n\mathbf{k}}) \quad (4)$$

(ii) the local density of states (LDOS), due to the orbital μ on the atom a, given by

$$N_{a,\mu}(E) = \frac{1}{N_w} \sum_{n,\mathbf{k}}^{N_w} |\langle a, \mu, \mathbf{R_i}|n, \mathbf{k}\rangle|^2 \delta(E - E_{n\mathbf{k}}) \quad (5)$$

(iii) the partial density of states (PDOS), due to the atomic species of type α (such as Cd, Se or Te atoms), given by

$$N_\alpha(E) = \sum_{a,\mu} N_{a,\mu}(E) \quad (6)$$

where the sum a runs over all sites of type α.

We emphasize that the $\mathbf{k}$-space integration carried in evaluating equations (4) and (5), is performed using the Monkhorst–Pack technique [18], and the δ-function is numerically approximated by a Gaussian:

$$\delta(x) = \frac{1}{\sigma\sqrt{2\pi}} \exp\left[-\frac{x^2}{2\sigma^2}\right] \quad (7)$$

of width $\sigma = 0.10$ eV to smear out the effects of finite size and consequently the discreteness of the Brillouin zone sampling and experimentally to take account of the thermal broadening. All the TDOSs are normalized to ten electrons (i.e. one atom).

(iv) The PDOSs are used to calculate the electric charge of individual atoms as follows:

$$q_\alpha = \frac{2e}{\rho} \int_{E_{\min}}^{E_F} N_\alpha(E)\, dE \quad (8)$$

where e is the electron charge; 2 stands for the re-normalization of density over a molecule rather than an atom; ρ is the atomic mole fraction (for instance in the case of $CdSe_xTe_{1-x}$ alloy, $\rho = 1$, x or $(1 - x)$ for Cd, Se or Te, respectively); $E_{\min}$ is any energy value below all state levels forming the TDOS; E_F is Fermi energy which is taken to be equal to $E_g/2$ as a frozen lattice state is assumed ($T = 0$ K).

3. Results and discussions

3.1. FCC bulk DOS

Figure 1 displays the calculated density of states for bulk (a) CdTe and (b) CdSe in their equilibrium face-centered cubic (FCC) crystal structures. The calculation uses the sp^3s^* TB basis set with spin–orbit interactions, whose parameters are from [14]. The valence-band edge (E_v) and the conduction-band edge (E_c) are indicated by the two vertical dashed lines. The VB edge is taken as the energy reference (i.e. $E_v = 0$). Each side of figure 1 shows the TDOS and PDOSs due to contributions from the constituent atoms. The bandgaps of both of these materials are direct at the BZ center (Γ-point) and their respective values are 1.60 and 1.78 eV at the frozen lattice state (0 K). As is well known, the bonds in both CdTe and CdSe are covalent with partial ionic character. For instance, by looking at the PDOSs, one can easily notice that the VB of the anion (like Te in figure 1(a) or Se in figure 1(b)) is much larger than the VB of the cation (like Cd in both figures 1(a) and (b)). In contrast, the conduction band (CB) of the cation is larger than that of the anion. Furthermore, the electronic charge of the Te VB, being a bit smaller than the one for Se, reveals the fact that Se is more electro-negative than Te (performing the integration of PDOS up to E_F yields 5.726 (e units) for the Te atom and 6.146 (e units) for the Se atom). One therefore expects that such mismatch in electro-negativity of anions would play a role in the bandgap bowing of alloys.

3.2. Ternary alloy DOS

Figure 2 displays the calculated DOSs for $CdSe_xTe_{1-x}$ ternary alloys with (a) $x = 0.25$, (b) $x = 0.50$ and (c) $x = 0.75$. The pair of dashed vertical lines refer to the VB and CB edges

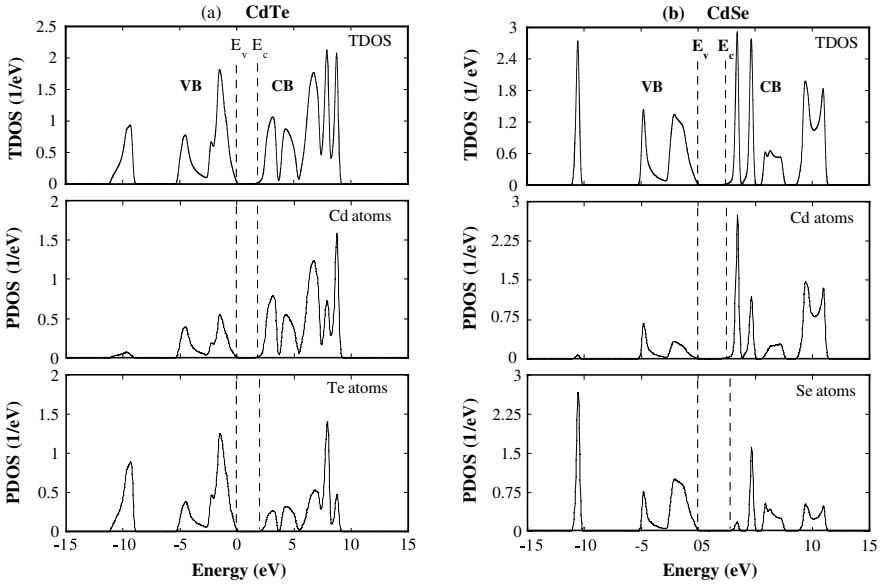

Figure 1. The total and partial density of states (TDOS and PDOS) calculated for zinc-blende structures of (a) CdTe and (b) CdSe.

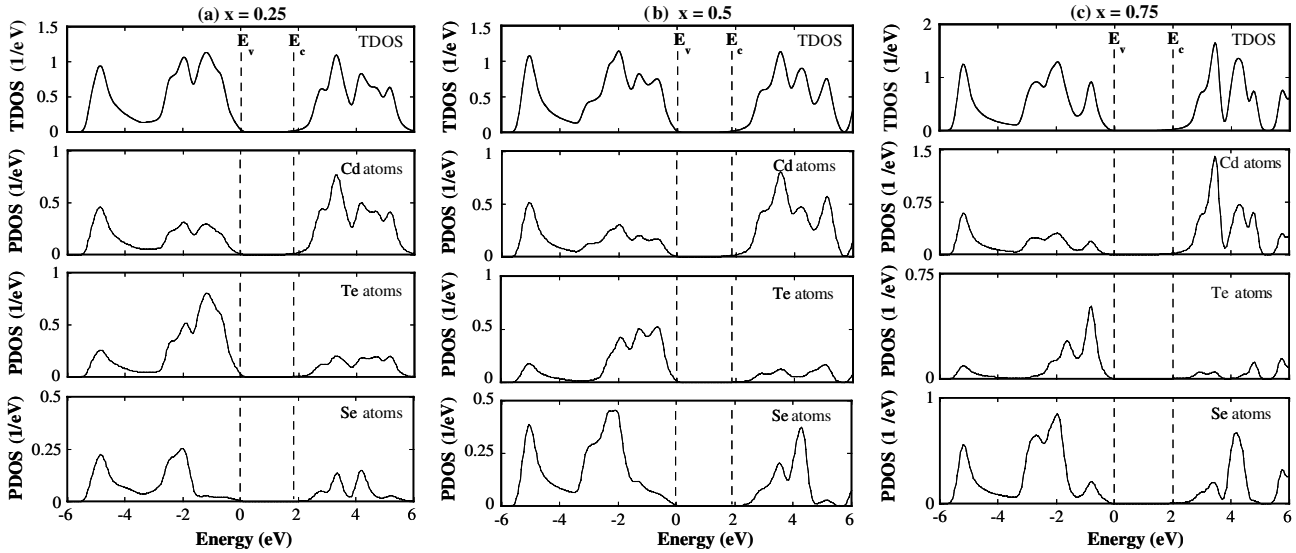

Figure 2. The TDOS and PDOS calculated for the common-cation $CdSe_xTe_{1-x}$ ternary alloys with (a) $x = 0.25$, (b) $x = 0.50$ and (c) $x = 0.75$.

(i.e. E_v and E_c, respectively). As in figure 1, the VB edge is taken as an energy reference (i.e. $E_v = 0$). In each part, we show TDOS in the upper panel and the PDOS contributions from Cd, Te, and Se as one moves lower in the consecutive panels. All DOSs are displayed for the energy range [−6, +6] eV in order to focus on the VB and CB states near the bandgap. First, in figure 2(a), one can notice a very interesting feature in the PDOS of Se atoms: the Se VB states are pushed down in energy away from the VB edge, as being more competitive than Te in accommodating more electrons. Since Se is more electro-negative, its corresponding VB states have a tendency to lie lower in energy than those associated with Te VB states. Consequently, the VB edge consists predominantly of states located on Te atoms. Second, in the same figure 2(a), one can also notice, through the PDOS, that Cd atoms are the largest contributors to the CB of the alloy. Consequently, the CB edge consists predominantly of states located on Cd atoms. Qualitatively, these features are persistent in the other two panels 2(b) and (c) when the Se mole fraction is increased.

The total charge of each individual atom is calculated by integrating the PDOSs up to the Fermi level, as described earlier, and the results are summarized in figure 3. One can notice that the charges of both Te and Se are varying around 6 while the charge of Cd varies around 2. This is consistent with the fact that the alloy constituent elements are from groups II and VI. More importantly, one can easily notice that the degree of ionicity of all the atoms increases linearly with Se density (x). The way in which the charge behaviors alter the bandgap bowing could be explained as follows. In the pure bulk states ($x = 0$ or 1) Se is more electro-negative than Te

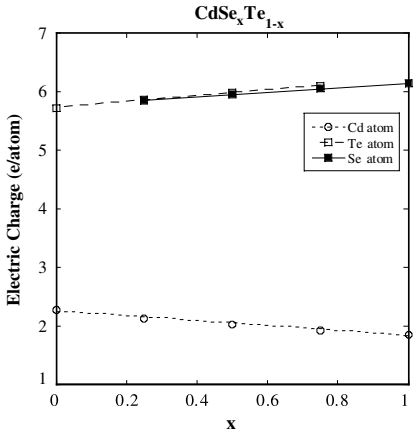

Figure 3. The calculated electric charges for the constituent atoms of the $CdSe_xTe_{1-x}$ ternary alloy versus mole fraction x.

and this is the cause of formation of a VBO $\simeq 0.5$ eV, with the VB edge of CdTe being higher than that of ZnTe. However, in the alloy state, the Se and Te are found to have comparable charges and compete to accumulate more charges (for instance, the charge of Te is even slightly higher than Se in the alloy state $0.25 \leqslant x \leqslant 0.5$ in figure 3). Such competition builds up a compromise in the charge confinements to accumulate on either Cd–Se or Cd–Te bonds and results in the bandgap bowing character of the alloys.

3.3. Modeling of experimental data

For the $CdSe_xTe_{1-x}$ ternary alloys, Campo and co-workers reported an experimental work [19] in which they made a clear comparison between their results of cathodoluminescence (CL) and photoluminescence (PL) for CdSeTe films grown on Si substrates using molecular-beam epitaxy (MBE). The Se mole fraction in their samples was determined by x-ray rocking-curve diffraction, wavelength-dispersive spectroscopy, and Rutherford back-scattering spectroscopy. These authors reported that the bandgaps (E_g) varied parabolically with composition as evidence of the bowing behavior in these alloys. Their PL data are shown in figure 4(a) as solid circles whereas CL data are open triangles. It should be emphasized that these measurements were done at room temperature (RT $\simeq$ 300 K), where the bandgap energy should be smaller than the frozen lattice case [20]. For this reason, in our theoretical modeling, we have made a minor change in one of the TB parameters (E_s^c) to yield the proper RT bulk bandgap energies (e.g. E_g(CdTe) is lowered by 80 meV and E_g(CdSe) is lowered by 40 meV). For the $CdSe_xTe_{1-x}$ alloys, the calculations are carried out for $x = 0.25$, 0.5, and 0.75 and the results are shown by open squares. We have performed a nonlinear fitting to both the experimental and theoretical data using the parabolic function

$$E_g = xE_g^{CdSe} + (1-x)E_g^{CdTe} - bx(1-x) \qquad (9)$$

where b is the bowing parameter. The results for E_g and b are summarized in table 1. For the PL data, we found that $b = 0.916$ eV while for the TB calculations we found that $b = 0.904$ eV. This excellent agreement made our claim valid while we recall that the calculations still rely on the validity of the VCA.

For the $ZnSe_{1-x}Te_x$ ternary alloys, Seong and co-workers [11] reported wavelength-modulated reflectivity and Raman characterization of single crystals grown by the vertical gradient freezing technique. The PL measurements were done at low temperatures (8 K) and the results are shown on figure 4(b) by solid triangles. At higher temperatures (room temperature, 'RT'), on the other hand, Chang and co-workers [21] reported investigations of a set of II–VI ternary alloys, among which they studied the $ZnSe_{1-x}Te_x$ alloys. The latter alloys were grown using MBE on GaAs substrates and were characterized using PL, CL, and high-resolution x-ray diffraction measurements. The bowing character was well observed in their data, which is displayed in figure 4(b) by open circles. In another related experimental work, reported by Wu and co-workers [22], the $ZnSe_{1-x}Te_x$ alloys were grown by MBE and characterized using photomodulated reflectivity, optical absorption, and PL spectroscopies at RT. Their data [22] also represented further evidence for bandgap bowing in these alloys and are shown as solid circles in figure 4(b). The bowing character has also been corroborated by the TB calculations,

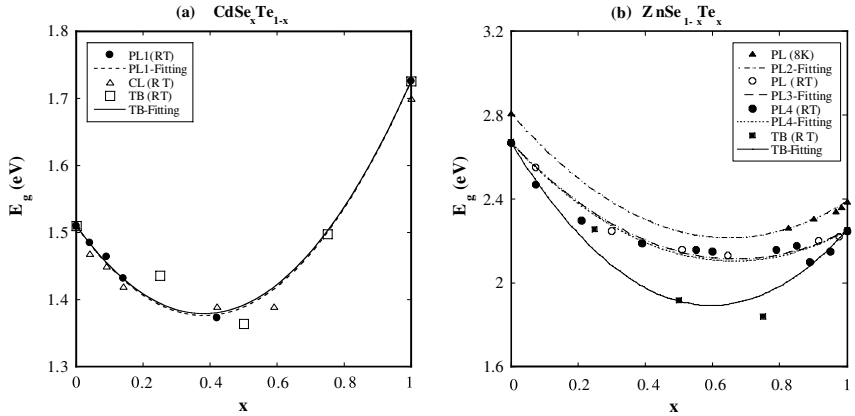

Figure 4. The variation of E_g with composition for (a) $CdSe_xTe_{1-x}$ and (b) $ZnSe_{1-x}Te_x$ ternary alloys. The photoluminescence data PL1, PL2, PL3, and PL4 correspond to [19], [11], [21], and [22] respectively, while CL is due to [19].

the results of which are shown in figure 4(b) by solid squares. All the curves in figure 4(b) display parabolic fitting to the corresponding experimental and theoretical data. Comparing the data presented in figure 4(b), one may make the following remarks: (i) the experimental bowing parameter is a bit higher at low temperatures [11]; (ii) the bowing parameters at RT of the experimental works of [21] and [22] are in excellent agreement; (iii) the TB bowing parameter, calculated to simulate the RT data, was found to be large. Although the TB bandgaps are smaller than the experimental ones, they represent the highest possible estimates that one can obtain by varying the VBO. They correspond to an overestimate of VBO of 1.2 eV. The TB results yield an overestimated bowing parameter b, but it is still smaller than what was reported in [10]. Possible reasons for such over-estimation could be the following: (1) lack of exact TB parametrization in the case of alloys away from the dilute regime; (2) deviation from the VCA, which is more pronounced in the case of the mid-alloy regime; (3) neglect of exciton effects in the TB scheme. Beyond these, the TB calculation is still capable of predicting the experimental bandgap bowing in $ZnSe_{1-x}Te_x$ alloys and to closely estimate their bandgaps in the dilute regime.

Table 1 summarizes the results of lattice mismatch ($\Delta a/a_0$), VBO, and bowing parameter (b) for the studied ternary alloys. One can observe that bandgap bowing exists in the common-cation ternary alloys and increases with the increase of VBO and lattice mismatch.

4. Conclusions

The electronic band structures of the common-cation $CdSe_xTe_{1-x}$ and $ZnSe_{1-x}Te_x$ ternary alloys were investigated using the sp^3s^* tight-binding method with the inclusion of spin–orbit coupling. In agreement with the experimental data, the bandgap energy is shown to have a bowing behavior as a function of composition. The *bowing* parameter is found to increase with VBO and lattice mismatch.

In the alloy state, the anions (Se and Te) are found to compete in trapping charges. Such competition builds up a compromise in the charge distribution among the alloy bonds and should be the main reason for the observed bandgap *bowing* character.

Acknowledgment

The authors are indebted to Dr Najeh Jisrawi for several fruitful discussions.

References

[1] For a review, see for instance Kolodziejski L A, Gunshor R L and Nurmikko A V 1995 *Annu. Rev. Mater. Sci.* **25** 711
[2] Trager-Cowan C, Parbrook P J, Henderson B and O'Donnell K P 1992 *Semicond. Sci. Technol.* **7** 536
[3] Taniguchi S *et al* 1996 *Electron. Lett.* **32** 552
[4] Nakamura S *et al* 1997 *Appl. Phys. Lett.* **70** 1417
[5] Van Vechten J A and Bergstresser T K 1970 *Phys. Rev.* B **1** 3351
[6] Bernard J E and Zunger A 1987 *Phys. Rev.* B **36** 3199
[7] Shan W, Walukiewicz W, Ager J W, Haller E E, Geisz J F, Friedman D J, Olson J M and Kurtz S R 1999 *Phys. Rev. Lett.* **82** 1221
[8] Kobayashi A, Sankey O F and Dow J D 1982 *Phys. Rev.* B **25** 6367
[9] Tit N and Al-Zarouni A 2002 *J. Phys.: Condens. Matter* **14** 7835
[10] García A E, Camacho A, Navarro H, Olguín D and Baquero R 2000 *Rev. Mex. Fis.* **46** 249
[11] Seong M J, Alawadhi H, Miotkowski I, Ramdas A K and Miotkowska S 1999 *Solid State Commun.* **112** 329
[12] El-Haj Hassan F, Hashemifar S J and Akbarzadeh H 2006 *Phys. Rev.* B **73** 195202
[13] Charifi Z *et al* 2005 *J. Phys.: Condens. Matter* **17** 7077
[14] Olguín D and Baquero R 1995 *Phys. Rev.* B **51** 16891
[15] Vögl P, Hjalmarson H P and Dow J D 1983 *J. Phys. Chem. Solids* **44** 365
[16] Tit N 2006 *J. Phys. D: Appl. Phys.* **39** 2514
[17] Wei S-H and Zunger A 1998 *Appl. Phys. Lett.* **72** 2011
[18] Monkhorst H J and Pack J P 1976 *Phys. Rev.* B **13** 5188
[19] Campo E, Hierl T and Hwang J 2004 *Proc. SPIE* **5564** 86
[20] Harrison W 1980 *Electronic Structure and Properties of Solids: the Physics of Chemical Bonds* (San Francisco, CA: Freeman)
[21] Chang J H, Cho M W, Makino H, Sekiguchi T and Yao T 1999 *J. Korean Phys. Soc.* **34** S4
[22] Wu J *et al* 2003 *Phys. Rev.* B **67** 035207